

# REPORT DOCUMENTATION PAGE

Form Approved  
OMB NO. 0704-0188

Public Reporting burden for this collection of information is estimated to average 1 hour per response, including the time for reviewing instructions, searching existing data sources, gathering and maintaining the data needed, and completing and reviewing the collection of information. Send comment regarding this burden estimates or any other aspect of this collection of information, including suggestions for reducing this burden, to Washington Headquarters Services, Directorate for Information Operations and Reports, 1215 Jefferson Davis Highway, Suite 1204, Arlington, VA 22202-4302, and to the Office of Management and Budget, Paperwork Reduction Project (0704-0188), Washington, DC 20503.

1. AGENCY USE ONLY (Leave Blank)		2. REPORT DATE	3. REPORT TYPE AND DATES COVERED <i>Final</i> <i>01 Jul 00 - 30 Jun 04</i>	
4. TITLE AND SUBTITLE <b>An Integrated Tunable Laser Cavity Sensor for Immunoassay Analysis and Molecular Diagnostics</b>			5. FUNDING NUMBERS DAAD19-00-1-0400	
6. AUTHOR(S) Carl Meinhart, Dan Cohen, Nelle Slack, Marin Sigurdson, Kimberly Turner, Larry Coldren				
7. PERFORMING ORGANIZATION NAME(S) AND ADDRESS(ES) University of California, Santa Barbara, CA 93111 BioCentrx, 1600 Bristol Ave. Culver City, CA			8. PERFORMING ORGANIZATION REPORT NUMBER <b>41398-LS</b>	
9. SPONSORING / MONITORING AGENCY NAME(S) AND ADDRESS(ES)  U. S. Army Research Office P.O. Box 12211 Research Triangle Park, NC 27709-2211			10. SPONSORING / MONITORING AGENCY REPORT NUMBER  <i>41398.11-LS</i>	
11. SUPPLEMENTARY NOTES The views, opinions and/or findings contained in this report are those of the author(s) and should not be construed as an official Department of the Army position, policy or decision, unless so designated by other documentation.				
12 a. DISTRIBUTION / AVAILABILITY STATEMENT  Approved for public release; distribution unlimited.			12 b. DISTRIBUTION CODE	
13. ABSTRACT (Maximum 200 words)  The current research is focused in two major areas: integrated laser design & development and microfluidic channel design with ac electrokinetic transport. We have modified the integrated laser design to make the waveguide symmetric. This allows for greater coupling between the laser sensor and the assay, and improves sensitivity by two orders of magnitude. The integrated sensor could measure up to 100 femtogram resolution. By tagging a latex bead to the analyte, the sensor can approach single molecule sensitivities. AC electrokinetically-driven microscale fluid and particle motion have been investigated for microfluidic design. We have focused on two mechanisms of sensor enhancement: AC fields can produce fluid circulation, for example through electrothermal forces, to enhance analyte motion towards ligands immobilized on the laser sensors. Additionally, AC fields can produce forces on particles directly, through dielectrophoresis (DEP), for concentration of analyte near the sensor. These two phenomena are investigated using numerical simulations. The results indicate that sensitivity and response time can be improved by nearly an order of magnitude for diffusion-limited reactions. This work is continuing with support from ARO through the Institute for Intercolaborative Biotechnology (ICB). We are also working with Dr. Nick Fell's group at ARL in Adelphi, MD to transition the work to Army applications.				
14. SUBJECT TERMS BioFlips, DBR Lasers, Microfluidics, AC electrokinetics, MEMS, Lab on a Chip			15. NUMBER OF PAGES <b>16</b>	
			16. PRICE CODE	
17. SECURITY CLASSIFICATION OR REPORT UNCLASSIFIED	18. SECURITY CLASSIFICATION ON THIS PAGE UNCLASSIFIED	19. SECURITY CLASSIFICATION OF ABSTRACT UNCLASSIFIED	20. LIMITATION OF ABSTRACT UL	

NSN 7540-01-280-5500

Standard Form 298 (Rev. 2-89)  
Prescribed by ANSI Std. Z39-18  
298-102

REPORT DOCUMENTATION PAGE (SF298)  
(Continuation Sheet)

1. List of Publications

2003 - 2004

(a) Manuscripts Submitted

C. S. Wang, J. A. Nolde, D. D. Lofgreen, L. A. Coldren, D. A. Cohen, "A self-aligned process to monolithically integrate a quasi-symmetrical sensing waveguide to a diode laser chemical sensor," submitted to *Applied Physics Letters*, 2004.

(b) Peer-reviewed Publications

D. A. Cohen, J. A. Nolde, A. Tauke Pedretti, C. S. Wang, E. J. Skogen, L. A. Coldren, "Sensitivity and scattering in a monolithic heterodyned laser biochemical sensor," *IEEE Journal of Selected Topics in Quantum Electronics*, vol. 9, pp.1124-1131, 2003.

C.D. Meinhart, D. Wang & Kimberly Turner, 2003 Measurement of ac electrokinetic flows, *J. Biomedical Microdevices*, 5(2), 139-145

Wang, D., M. Sigurdson, et al. (2004). "Experimental Analysis of Particle and Fluid Motion in AC Electrokinetics." accepted Experiments in Fluids.

(c) Non-peer-reviewed Publications

C. S. Wang, D. A. Cohen, J. Nolde, D. D. Lofgreen, and L. A. Coldren, "A diode laser chemical sensor utilizing an oxidized lower cladding layer for high sensitivity," submitted to the IEEE LEOS annual meeting, November 2003.

Sigurdson, M., C. D. Meinhart, et al. (2003). AC Electrokinetics for Microfluidic Immunosensors. 2003 ASME International Mechanical Engineering Congress and Exposition, Washington, D.C., ASME.

Sigurdson, M., C. D. Meinhart, et al. (2003). Biosensor Performance Enhancement Through AC Electrokinetics. Micro TAS'03, Squaw Valley, CA.

Sigurdson, M., C. D. Meinhart, et al. (2004). AC Electrokinetic Stirring for Microfluidic Bio-Sensors. Volume IV Biomeolecular Sensing, Processing and Analysis. R. Bashir and S. T. Wereley, Kluwer. IV.

Wang, D., C. D. Meinhart, et al. (2003). Two-Color Micro PIV Measurements of Particle and Fluid Motion in AC Electrokinetics. 2003 ASME International Mechanical Engineering Congress and Exposition, Washington, D.C., ASME.

Wang, D., M. Sigurdson, et al. (2004). Application of PIV to AC Electrokinetic Flows. Particle Image Velocimetry: Recent Improvements Proceedings of the EUROPIV 2 workshop. M. Stanislas, J. Westerweel and J. Kompenhans, Springer-Verlag.

Wereley, S. T. and C. D. Meinhart (2004). Electrokinetics in Microdevices. Complex Systems Science in BioMedicine. Deisboeck, Kresh and Kepler. New York, Kluwer Academic - Plenum Publishers.

(d) Presentations

NA

2002

(c) Non-peer-reviewed Publications

M. Sigurdson, C. D. Meinhart, D. Wang, X. Lui, J. Feng, S. Krishnamoorthy, V.B. Makhijani. 2002. Transport Enhancement in Tunable Laser Cavity Sensor. ASME – IMECE'02 MEMS Symposium, New Orleans, LA, Nov. 17–22.

D. A. Cohen, E. J. Skogen, J. Nolde, and L. A. Coldren "Sensitivity and scattering in an integrated heterodyned laser biochemical sensor," presented at the 18<sup>th</sup> IEEE International Semiconductor Laser Conference, Garmisch, Germany, September 29 – October 3, 2002.

2001

(b) Peer-reviewed Publications

D. A. Cohen, E. J. Skogen, H. Marchand, L. A. Coldren, "Monolithic chemical sensor using heterodyned sampled grating DBR lasers", *Electronics Letters*, 37, 1359, 2001.

(c) Non-peer-reviewed Publications

D. A. Cohen, E. Skogen, J. Nolde, D. Tung, L. A. Coldren, "A monolithic chemical sensor using tandem heterodyned Sampled Grating SBR lasers", *presented at IEEE LEOS 2001 Annual Meeting, San Diego, CA, 11-15 November 2001, paper TuM4.*

C. D. Meinhart, D. Wang 2001 Accurate Measurement of Dielectrophoretic (DEP) Mobility of particles and macromolecules, *Proceedings of  $\mu$ -TAS 2001, Monterrey, CA.*

M. Sigurdson, C. D. Meinhart, K. Turner, L. Coldren, D. Cohen, T. Stultz, & N. Slack 2001 An integrated SGDBR laser-based biosensor, *Proceedings of  $\mu$ -TAS 2001, Monterrey, CA.*

## 2. Demographic Data for Reporting Period

(a) Number of Manuscripts Submitted - 2

(b) Peer-reviewed Publications - 2

(c) Non-peer-reviewed Publications - 7

(d) Presentations - 0

## 3. Demographic Data for life of this agreement

(a) Number of Scientists Supported by this agreement - 10

### Integrated Laser Development

Dan Cohen, Ph.D., Research Engineer, ECE, UCSB

Jill Nolden, Graduate Student, ECE, UCSB

Erik Skogen, Graduate Student, ECE, UCSB

Larry Coldren, Ph.D., Professor, ECE, UCSB

### Biochemistry Development

Nelle Slack, Ph.D., Research Scientist, ThauMDx

Anatoly Rivlin, Ph.D., Research Scientist, ThauMDx

### Microfluidic Design

Carl Meinhart, Ph.D., Associate Professor, MEE, UCSB

Kimberly Turner, Ph.D., Assistant Professor, MEE, UCSB

Marin Sigurdson, Research Engineer, MEE, UCSB

Michael Northen, Graduate Student, MEE, UCSB

(b) Number of Inventions – 3

(c) Number of PhDs awarded – 3 (in progress)

(d) Number of Bachelor Degrees awarded as a results – 0

(e) Number of Patents Submitted – 2

(f) Number of Patents Awarded – 0 (2 under consideration)

(g) Number of Graduate Students Supported – 3

(h) Number of FTE Grad Students supported – 3

(i) Number of Post Doctorate Students supported – 2

(j) Number of FTE Post Doctorate students supported – 2

(k) Number of Faculty supported by this agreement – 3

(l) Number of other staff supported by this agreement – 2

(m) Number of Undergrads supported – 1

(n) Number of Master Degrees awarded – 0

### 3. Report of Inventions

“Electrokinetic Concentrator for Immunoassays,” M. Sigurdson, Xiaojin Liu, C. D. Meinhart, Invention Disclosure submitted to UC Office of Technology.

“An Integrated Chemical Sensor,” C. D. Meinhart, L. Coldren & T. Stultz, Patent Pending.

“Method for increased sensitivity in evanescent field immunoassays,” D. Cohen, N. Slack, & J. Pawlak, University of California Technology Transfer Office.

### 4. Scientific Progress

#### 4.1 Major Milestones:

##### 1. Laser Development

1.1	Modeling and design	Completed
1.2	Growth and fabrication	Completed
1.3	DBR lasers	Completed
1.4	Flip-chip technology	Completed
1.5	Integrated laser/ heterodyne detector	Completed

##### 2. Microfluidic Analysis / Fabrication

2.1	Microfluidic channel design (passive) –	Completed
2.2	Microchannel design (DEP)	Completed
2.3	Fabrication of microchannels	Completed
2.4	Simulation of DEP transport	Completed
2.5	Simulation of DEP electrodes	Completed
2.6	Fabrication of DEP device	Completed
2.7	Establish optimal flow parameters for maximum sensitivity -	Completed
2.8	Characterization of fluid flow over TLCS	Completed

##### 3. Biochemistry development

3.1	Develop methodology for depositing molecules on InP –	Completed
3.2	Develop methodology for selective immobilization on InP –	Completed

#### 4.2 Integrated Laser Development (Dan Cohen)

##### 4.2.1 Initial Design

Our proposal outlined a Y-branch waveguide geometry to combine the light from the reference and sensing lasers, and direct the light to a photodetector. Results from a similar structure fabricated within the context of another program indicate that the long curving waveguides have considerable loss and are difficult to fabricate. We have designed a simpler geometry, consisting of a wide multimode interference coupler with a photodetector within the coupler itself. The geometry is shown schematically in Fig. 1, and the beam propagation simulation in Fig. 2 shows how the field from one waveguide input migrates to the middle of the coupler in a distance of only 200 microns. The waveguide from the second laser is placed at the opposite edge of the coupler, so the fields would overlap in the center of the coupler. A small, high-speed detector is integrated at this point of overlap.

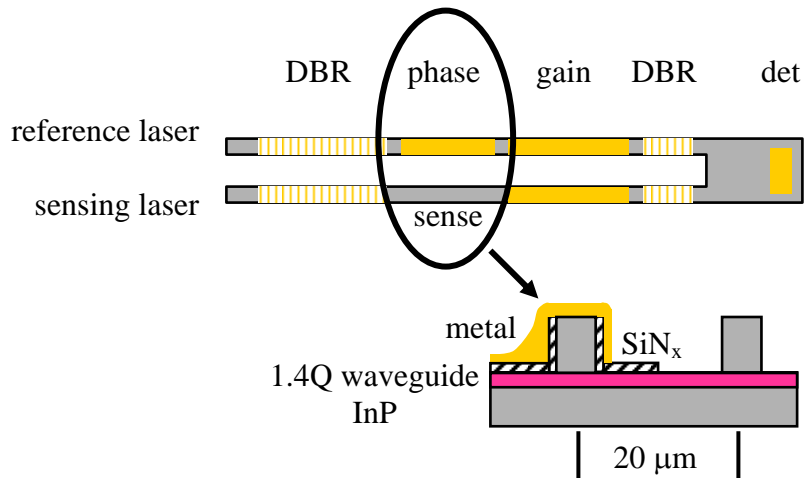


Figure 1. Schematic of the tunable laser cavity sensor, based on sampled grating distributed Bragg reflector (SGDBR) lasers. DBR mirrors, phase control, and laser gain sections are shown, along with a field combiner and integrated detector.

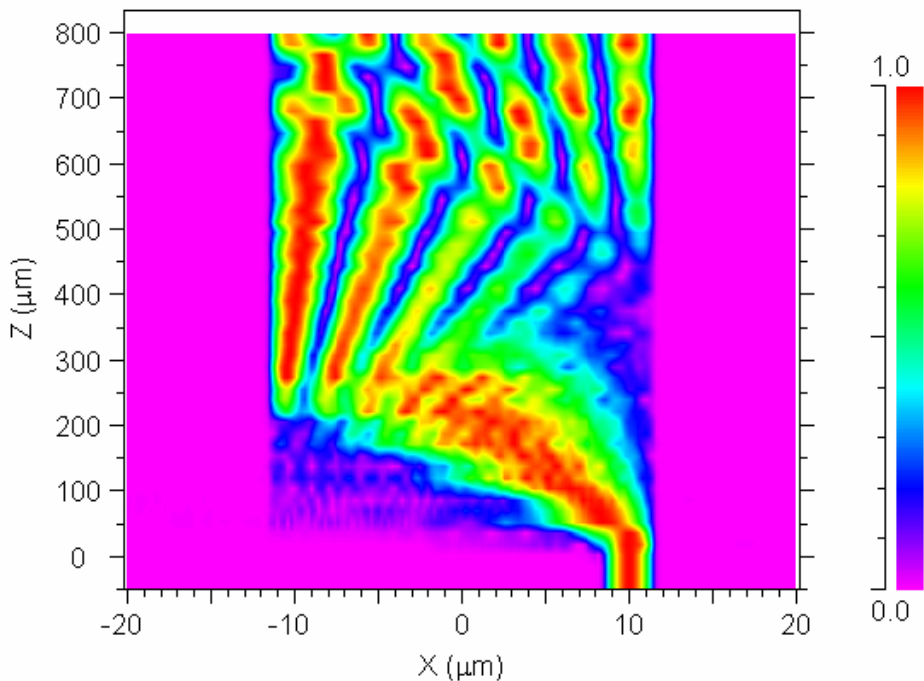


Figure 2. Beam propagation simulation of the multimode interference coupler. Light from one laser waveguide enters at the lower right, and propagates to the center of the waveguide after 200 microns. Light from the second laser enters from the opposite side (not shown), and a detector integrated in the region of overlap detects the heterodyne signal

The TLCS was first demonstrated using the structure shown in Fig. 1. Tandem sampled-grating distributed Bragg reflector (SGDBR) lasers were used, with a simple planar waveguide beam combiner and an imbedded photodiode for heterodyne detection. Details of the device may be found in Cohen *et al.* (03). The sensor was characterized by measuring the response to different alcohol mixtures, as shown in Fig. 3. The shift in heterodyne frequency varied nearly linearly with the index of refraction of the analyte. Also shown is the phase section current required to maintain a constant heterodyne frequency, showing that the sensor may be operated in a closed-loop fashion, which provides a superior dynamic range and improved signal-to-noise ratio. The

heterodyne signal linewidth varied inversely with laser power, as expected, and reached a minimum value of 15 MHz (Cohen et al., 03). The response to temperature variations is an important issue, particularly for field applications. Since the heterodyne signal measures the difference in optical frequencies between two nearly identical lasers, we expect good rejection of temperature drift. Indeed, the heterodyne frequency was found to drift with temperature at only 1/100 the rate at which the individual lasers drifted (Cohen *et al.*, 01.)

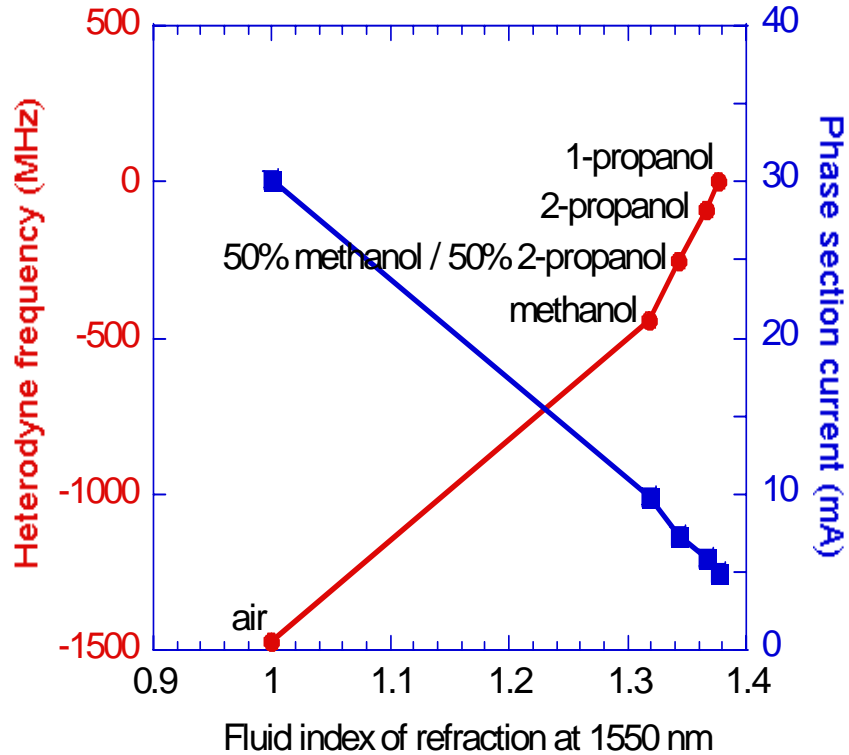


Figure 3. Heterodyne frequency shift versus analyte index of refraction. Also shown is the reference laser tuning current needed to maintain a constant heterodyne frequency, for use in a feedback circuit.

#### 4.2.2. Design Revision for Sensitivity

A detailed analysis of the data shown in Fig. 3 revealed that the sensitivity was limited by the poor overlap between the optical field and the analyte. Indeed, in the standard ridge waveguide shown in Fig. 4(a), the overlap is only a few hundredths of a percent, and cannot be increased significantly by changing the ridge dimensions. However, by removing the high refractive index substrate to form the channel waveguide shown in Fig. 4(b), a hundredfold improvement in the mode overlap could be achieved.

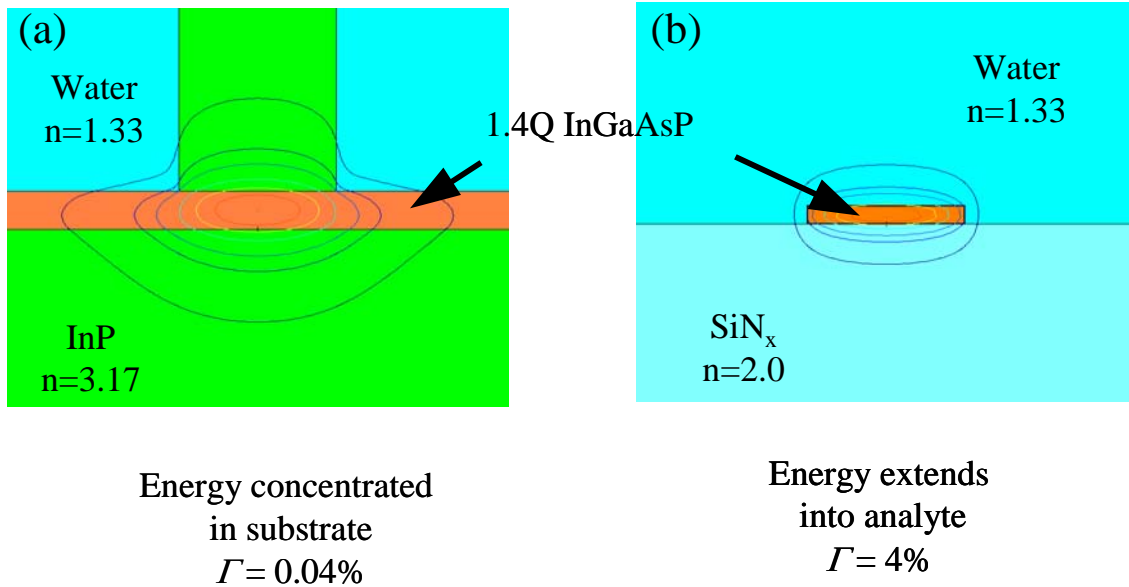


Fig. 4. Optical mode overlap with the analyte for (a) ridge waveguide and (b) channel waveguide.

If such a structure could be incorporated into the sensing region of the TLCS, the resulting sensitivity would be as shown in Fig. 5. Assuming a heterodyne frequency resolution of 1 MHz, a bound mass as low as 100 femtograms could be detected, corresponding to  $10^5$  average-sized protein molecules. If “mass-tags” such as latex beads or silicon nanospheres were conjugated to the target molecules, the sensitivity could be improved to the single-molecule range.

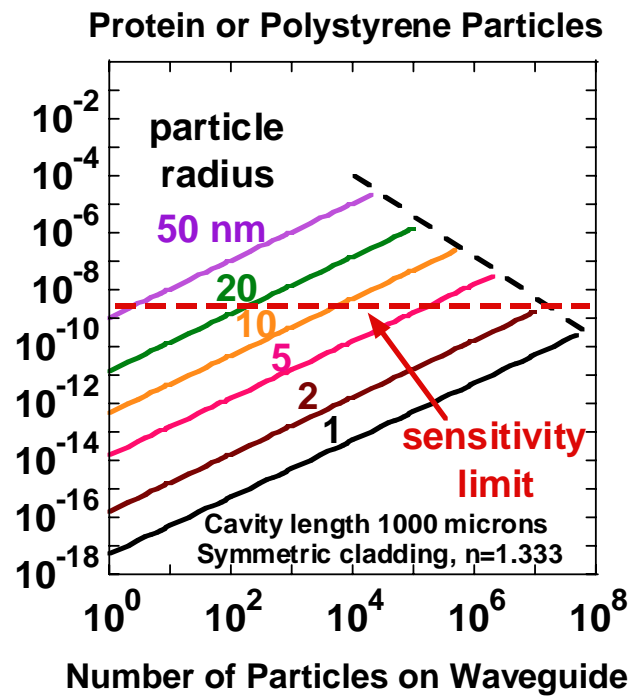


Figure 5. TLCS sensitivity, assuming a channel waveguide sensing region.

#### 4.2.3 High Sensitivity Waveguide Fabrication

It is not easy to implement index matched structure shown in Fig. 4b. We have pursued two approaches. The first is to use a selective chemical etchant to remove the InP below the waveguide, and then

replace it with a polymer for mechanical support. Unfortunately, this requires orienting the laser along a  $\langle 100 \rangle$  crystal direction to avoid defining  $\langle 111 \rangle$  stop etch planes. This orientation, in turn, complicates the epitaxial regrowth used in our standard SGDBR laser process. It also eliminates the possibility of using cleaved facets. This latter point is not a serious problem, since ultimately we won't need to couple light off the chip. Fig. 4 shows a waveguide test structure that has been undercut seven microns and then supported by a thick photoresist layer. The two overhanging layers are InGaAs, with a thin intervening InP layer also etched away. We ultimately decided this approach was not viable for the reasons given above.

The second approach, which we ultimately used, involves the fabrication of a novel coupled-cavity sensor that utilizes wet oxidation to convert a high index semiconductor layer into a low-index oxide layer. The device is shown in Fig. 7, and is described in detail in (Cohen *et al.*, 01; Wang *et al.*, 04). This device consisted of a Fabry Perot laser integrated with a simple waveguide etalon, such that changes in the refractive index of the medium surrounding the etalon resulted in a shift of the envelope of lasing modes. The wavelength shift is shown in Fig. 8, as a function of the analyte index of refraction. Analysis of this data shows that the mode overlap with the analyte was increased to nearly 5%, verifying the predicted hundred-fold improvement.

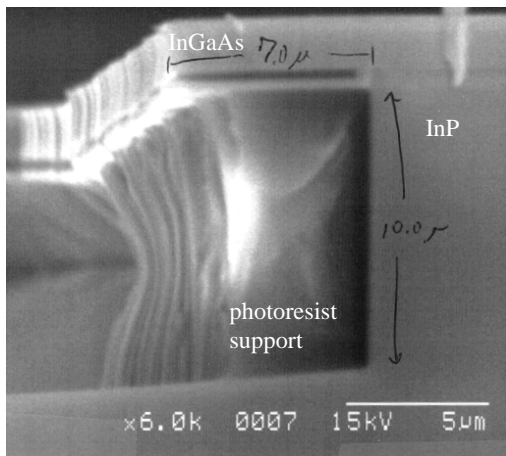


Figure 6. Test structure showing selective removal of an InP layer below an InGaAs layer, and mechanical support with a low index dielectric (photoresist here.) This method ultimately was determined not viable

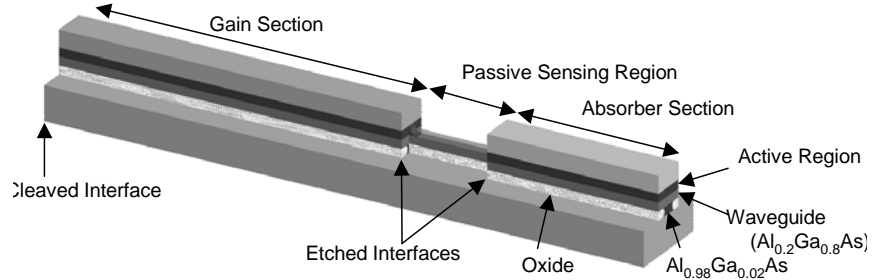
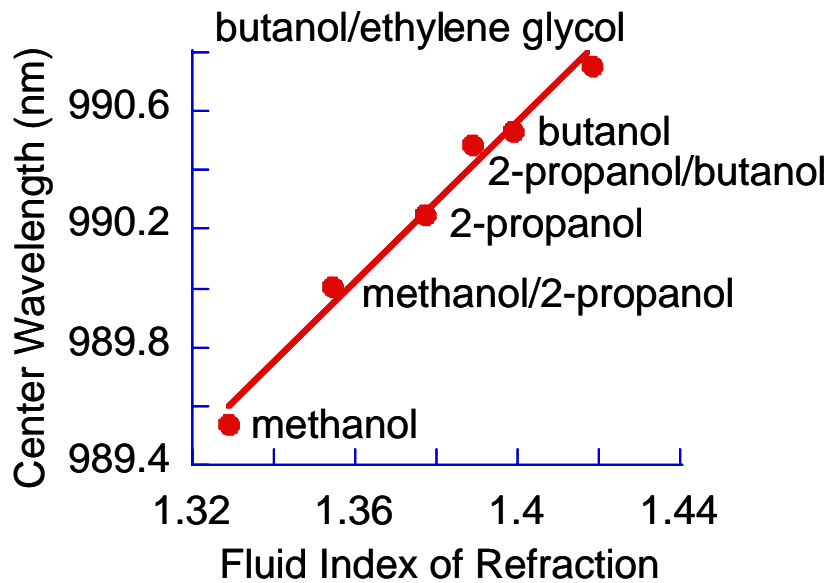
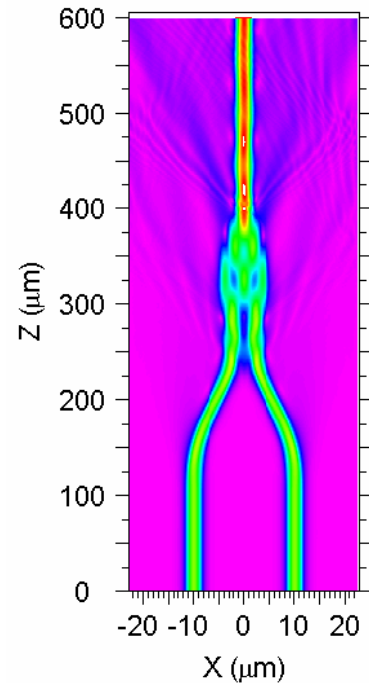


Figure 7. Schematic of the coupled cavity laser sensor with semiconductor converted to low index oxide layer for index matching as in Fig. 6.



**Figure 8.** Wavelength shift of envelope of lasing modes, as a function of analyte index of refraction.



**Figure 9.** Beam propagation simulation of a field combiner consisting of curved waveguides and a short multimode interference section

#### 4.2.4 Design Revision for Heterodyne signal strength.

We used a simple slab waveguide field combiner in the first TLCS design. While this was easy to fabricate, and performed well enough to evaluate the sensitivity and stability issues, the signal strength was too low for practical use. In this combiner, the two optical beams fall on the detector at an angle, leading to a spatial fringe pattern across the width of the detector, which reduces the modulation depth of the heterodyne signal. We have designed a new field combiner to eliminate this problem, making use of newly developed waveguide fabrication techniques. The coupler incorporates both curved waveguides as in traditional Y-branch combiners, and a multimode interference coupler to eliminate fabrication difficulties associated with traditional Y-branch combiners. The beam propagation simulation shown in the Fig. 9 indicates that the new design is compact and low-loss. This was incorporated into the revised TLCS design described below.

#### 4.2.5 Design Revision for Control

Our first results were obtained with a TLCS that utilized sampled-grating DBR lasers that afford very wide wavelength tuning. While this feature provides higher dynamic range and some spectroscopic capability, wavelength control is complicated because several tuning currents must be controlled simultaneously. In developmental devices, we must also collect the light off-chip to bring the sensor and reference laser wavelengths close enough to obtain a heterodyne signal. These requirements complicate testing, so we developed a simpler *unsampled* DBR technology to include in the “workhorse” generation of devices.

#### 4.2.6 Flip Chip Integration

Arrays of six TLCS sensors were flip-chip bonded onto silicon microfluidic circuits (such as that shown in figure 10a), using gold bonding pads. An SEM micrograph of a bonded die is shown in Fig. 10b. Successful bonding of more than eighty contacts was achieved. The sensor was then characterized by pumping alcohols through the fluidic circuit, again showing a heterodyne frequency shift comparable to the results with bare die. However, a long lag was observed between the time the fluids were switched and the time the response was observed, as shown in Fig. 11, perhaps indicating poor flushing of the area adjacent to the sensing ridge waveguide.

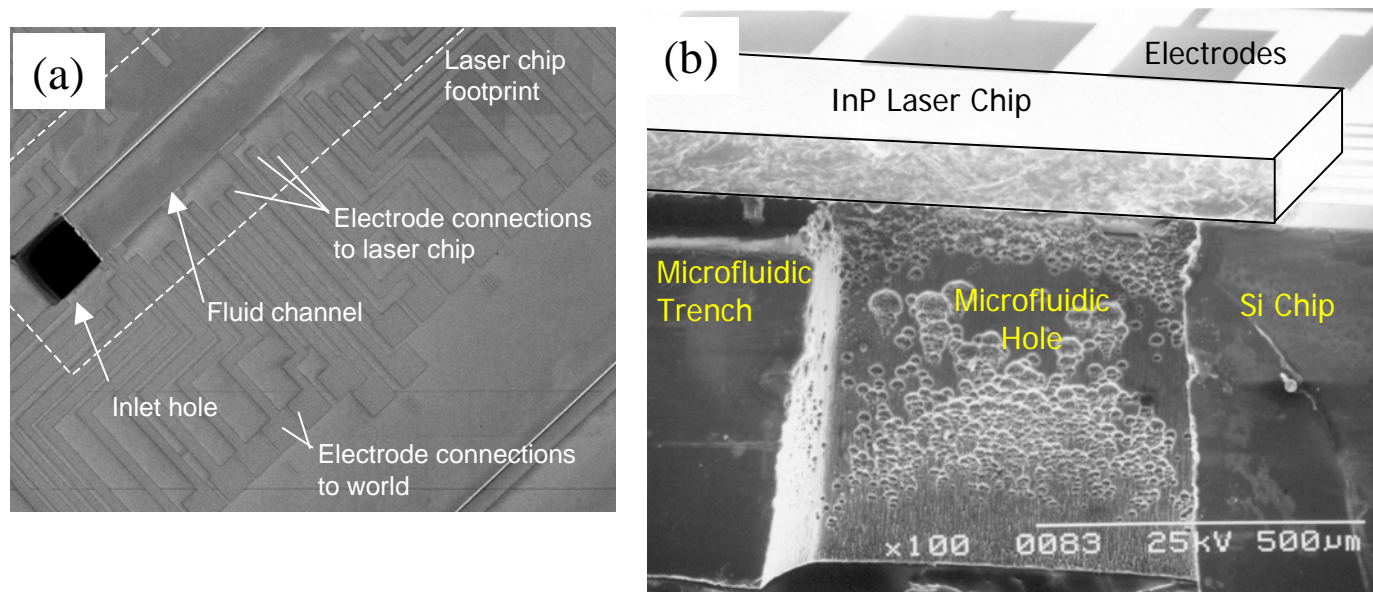


Figure 10. Silicon microfluidics chip (a) from above, before integration with with laser chip, and (b) from the side (cleaved to show interior), after flip-chip bonding with laser chip

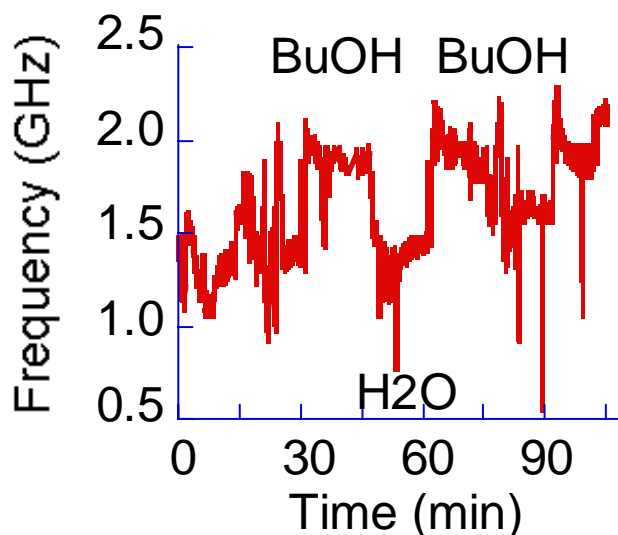


Figure 11. Response of the flip-chip bonded TLCS to changing analytes.

### 4.3 Microfluidics Development

We have explored using AC Electrokinetics for control of fluid and suspended particles and ultimately for binding enhancement. AC Electrokinetics refers to induced particle and/or fluid motion resulting from externally applied AC electric fields, and can be classified into three broad areas: dielectrophoresis (DEP), electrothermal forces, and AC electroosmosis. Electrothermal flow results from non-uniform temperature fields creating conductivity and permittivity gradients, which interact with the electric field to generate flow patterns near the electrodes. Electrothermal flow can create microscale stirring, thereby enhancing transport of analyte to the binding region of a biosensor.

#### 4.3.1 Wedge Simulations and Experiments

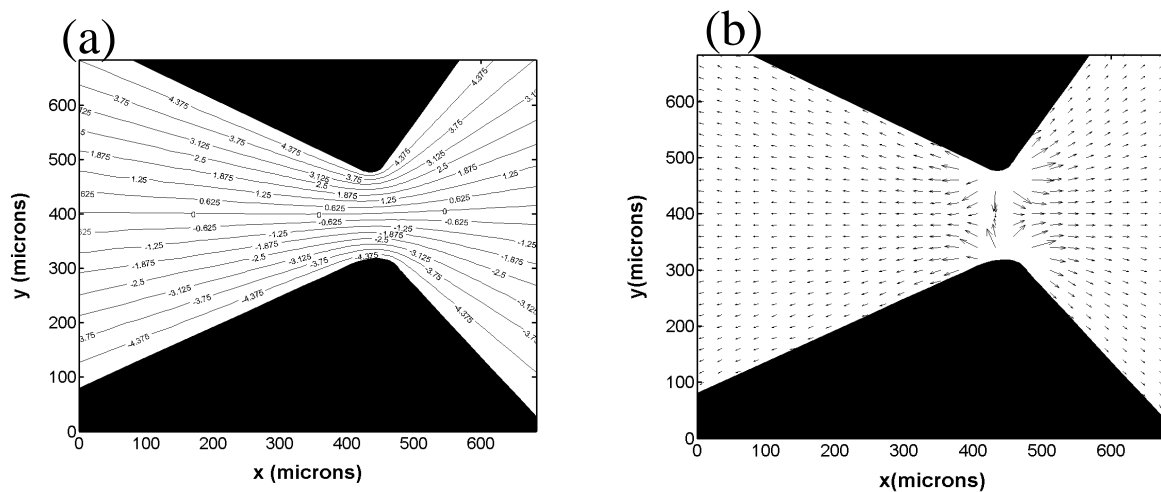
Micron-resolution Particle Image Velocimetry ( $\mu$ -PIV) was used to measure the motion of nominally 1- $\mu$ m diameter polystyrene particles suspended in a water/sugar solution in a microdevice. Particle motion is induced by an applied electric field through dielectrophoretic (DEP) forces and through viscous interactions with the fluid. The motion of the fluid is governed by electrothermal forces arising from temperature-induced

gradients in the electrical properties of the fluid near the electrodes and through the viscous interaction with the particles. Comparisons between finite element calculations and experimental micro-PIV results confirm quantitatively that electrothermal forces play a major role in the motion of the particles.

The goal is to use micron-resolution particle image velocimetry ( $\mu$ -PIV) to measure spatially and temporally resolved dielectrophoretic-induced motion of polystyrene particles and macromolecules in flowing microchannels (Meinhart et al., 1999). The results from these experiments reveal the DEP forces on particles as a function of their motion and spatial position. DEP has been used in a variety of BioMEMS applications, including sorting cancer cells and capturing DNA molecules (Yang et al., 1999; Miles et al., 1999). Most of the DEP force models simplify the particles to be either spheres or shells. In addition, the viscous drag force is usually modelled as a rigid sphere flowing through a uniform fluid. In many practical applications, such as transporting coiled DNA molecules through microchannels using DEP, these assumptions are not valid. In addition to DEP forces, electrothermal effects can create body forces on the fluid, which can cause the particle to move in a pattern inconsistent with DEP forces (Ramos et al., 1998).

The electric field was calculated in a wedge-shaped geometry by solving  $\nabla^2 V = 0$  using Femlab<sup>TM</sup> software. Fig. 12a shows the voltage potential in the wedge device. The DEP force is calculated by taking the gradient of the magnitude square of the  $E$ -field. The force field of  $F_{DEP}$  is shown in Fig. 6, for negative DEP. If the particles were only influenced by  $F_{DEP}$  and the fluid was stationary, then for steady conditions the DEP force would balance the viscous drag force, and the particle motion would follow the DEP force field shown in Fig. 12b. According to Ramos et al. (1999), it is also important to account for the electrothermal forces on the fluid. These forces are a result of temperature gradients produce by Joule heating of the fluid. The temperature gradients create gradients in the dielectric and conductivity properties of the fluid, which in the presence of an electric field create a localized body force on the fluid. The fluid motion due to electrothermal effects is estimated following Ramos et al. (1999), and is shown in Fig. 12c.

The trajectories of 1- $\mu$ m diameter polystyrene particles embedded in a 8.5% sucrose and 0.3% dextrose solution was measured in the wedge device. The device consisted of two brass electrodes sandwiched between two glass wafers. A voltage of 10V RMS at 10 kHz was applied to the electrodes. The Clausius-Mossotti factor is  $K=-0.5$  for the current conditions, producing a negative DEP force. The particle-velocity field is measured quantitatively using  $\mu$ -PIV and shown in Fig. 12d, following Meinhart et al. (1999). The velocity field is characterized by a saddle point at the center of the wedge, with four recirculating vortices. The motion of the particles closely resembles the motion of the fluid due to electrothermal effects. This indicates that electrothermal effects play a significant role in the fluid motion, and the particle motion through viscous coupling.



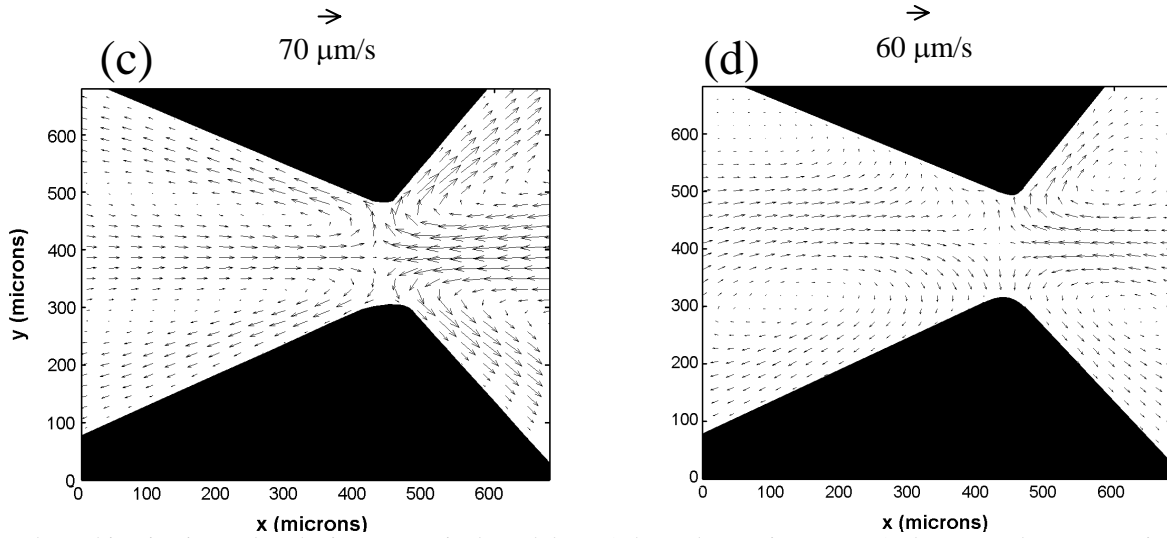


Figure 12. Electrokinetics in wedge device; numerical models (a & b) and experiments (c & d). (a). Voltage potential of the DEP wedge device calculated using Femlab™ software. (b) Negative gradient of the magnitude square of the electric field calculated using Femlab™ software. The vectors depict, to within a constant, the force field due to negative dielectrophoresis. (c) Velocity field of the fluid motion resulting from electrothermal forces (estimated using finite element simulation). (d) Micron-resolution PIV velocity field of 1- $\mu$ m dia. polystyrene particles under the influence of dielectrophoresis and viscous coupling to the underlying fluid motion.

#### 4.3.2 Microchannel Simulations

The finite element packages CFD-ACE+ (CFD Research Corp, Huntsville, AL) and FEMLAB (COMSOL AB, Stockholm, Sweden) were used to simulate electrothermally induced flow and subsequent enhanced binding at the Tunable Laser Cavity Sensor. First, the quasi-static potential field produced by two electrodes along the cavity wall subjected to an AC ( $\sim 100$ kHz) field is calculated (Fig. 13). Ignoring unsteady effects, and balancing Joule heating with thermal diffusion, a non-uniform temperature field is calculated (Figure 14). Gradients in temperature produce gradients in permittivity and conductivity in the fluid. These variations in electric properties produce gradients in charge density and perturb the electric field. Assuming the perturbed electric field is much smaller than the applied electric field, and that advection of electric charge is small compared to conduction, the time-averaged electrothermal force per unit volume for a non-dispersive fluid can be written as (Ramos, 1999)

$$\vec{F}_{ET} = -0.5 \left[ \left( \frac{\nabla \sigma}{\sigma} - \frac{\nabla \epsilon}{\epsilon} \right) \vec{E}_{rms} \frac{\epsilon \vec{E}_{rms}}{1 + (\omega \tau)^2} + 0.5 |\vec{E}_{rms}|^2 \nabla \epsilon \right] \quad (1)$$

The first term on the right hand side of Eq. (1) is the Coulombic force, and is dominant at low frequencies. The second term is the dielectric force, and is dominant at high frequencies. The crossover frequency scales inversely with the charge relaxation time of the fluid, and typically occurs at around several MHz.

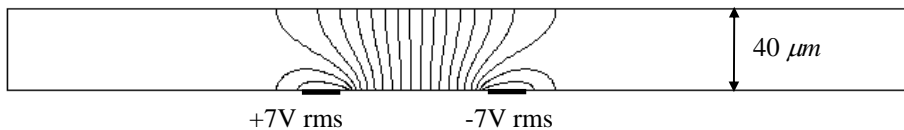


Figure 13. 2-D simulation of quasi-static electric potential contours in microchannel.

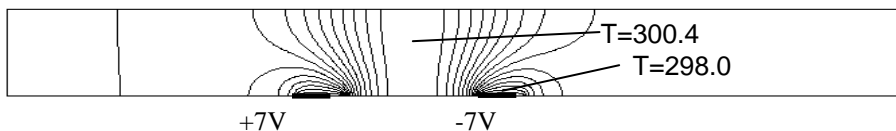


Figure 14. Temperature field contours generated by field in Figure 1. Metal electrodes act as heat sinks, removing heat from channel.

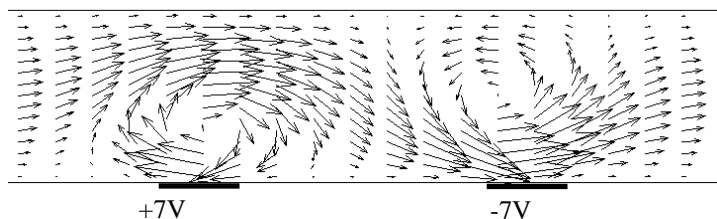


Figure 15. 2-D simulation of electrothermally enhanced velocity field in microchannel (center section only to show detail). 100  $\mu\text{m/s}$  pressure driven flow is enhanced by electrothermal flow generated by two electrodes along channel bottom. Electrothermal velocity is of order 300  $\mu\text{m/s}$ .

The electrothermal force shown in Eq. (1) is a body force on the fluid. The motion of the fluid can be determined by solving the Stokes' equation for zero Reynolds number fluid flow, and is shown in Figure 12. The velocity of the ETF is of order 300  $\mu\text{m/s}$ , and is characterized by a pair of counter rotating vortices. The fluid is convected with small eddy motions, which may effectively stir the analyte. If antibodies have been immobilized on the channel wall in a region of increased flow, these eddy motions will transport antigen to the antibody binding region.

We now investigate the effect these flow patterns may have on the binding response of the TLCs. The velocity field shown in Figure 15 suggests the most effective location of the electrodes is on the wall opposite the laser. The convective scalar equation subject to a first order binding boundary condition at the binding surface (equations given in Myszkowski, 98) predicts the suspended concentration of antigen within the microchannel. Figure 16a shows the binding nondimensionalized by the immobilized antibody concentration ( $R_T = 1.7 \text{ nM cm}$ ) for non-enhanced (0V) as well as enhanced (7V, 14V) microchannel flow. Often these assays are performed in a microarray rather than flow-through format. Figure 16b shows binding enhancement predictions for a similar geometry with zero net flow. In both cases, several factors increase in binding are predicted in the first 100 seconds.

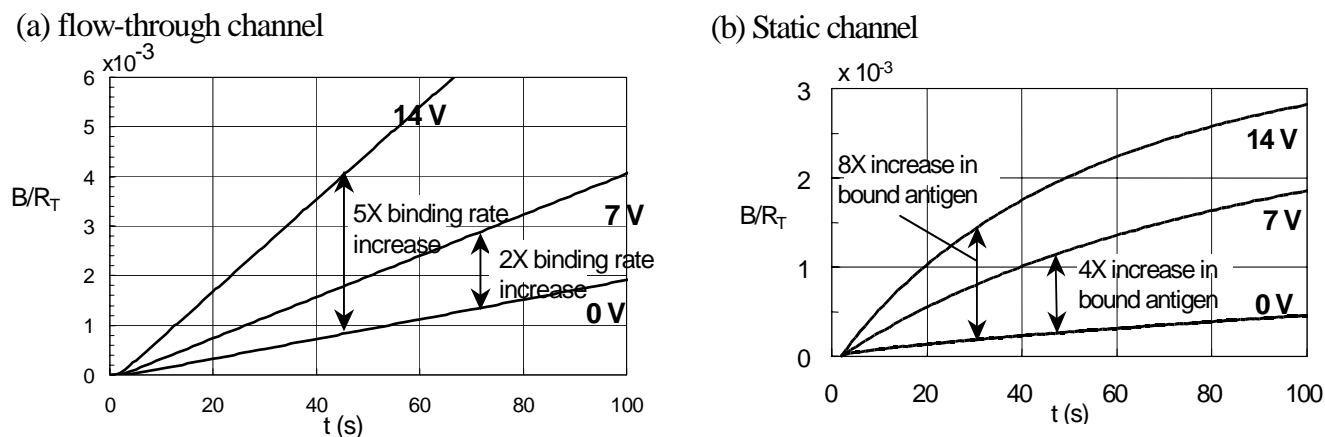


Figure 16: Numerical simulation of normalized bound antigen concentration, (a) in 40  $\mu\text{m}$  microchannel with inlet channel flow rate averaging 100  $\mu\text{m/s}$ . With 7V applied rms voltage, the binding rate is about double the non-enhanced binding rate. With 14 Vrms applied, the binding rate jumps to 5 times the non-enhanced rate. (b) in microcavity enhancement, with zero net flow. The differences in the two curves show an increase in binding rate which yields a factor of 4 higher binding for 7 V and a factor of 8 higher binding after 30 seconds for 14 V applied root-mean square potential. The binding improvement for the 14 V case decreases to around 6 X after 100 seconds: the binding is no longer completely transport-limited. These results suggest that electrothermally induced flow can significantly improve immunoassay performance by increasing binding rates

#### 4.3.3 Dielectrophoresis

Electrothermal stirring will increase binding rates if the assay is transport limited rather than reaction-rate limited. If, however, the binding is reaction limited, circulating the suspension will not speed up the assay. In such a case, concentrating the suspended analyte near the binder can improve binding rates. Dielectrophoresis, or DEP can effect this concentration. DEP is a force on particles in a non-uniform electric field arising from differences in dielectric properties between the particles and the suspending fluid. The time-averaged force on a homogeneous sphere can be approximated

$$F_{DEP}(x,y)=2\pi \varepsilon_m r_p^3 \operatorname{Re}\{K\} \nabla|E|^2 \quad (2)$$

Here  $\operatorname{Re}\{K\}$  is called the dielectrophoretic mobility and is the real part of  $K$ , the Clausius-Mosotti factor, which depends on the complex permittivity of particle and medium. Through this factor, the DEP force depends not only on the dielectric properties of the particle and medium, but also on the frequency of the applied field. Because of the dependence on the gradient of the electric field, DEP force dies off quickly with distance from an electrode array. Together with cubic dependence on particle radius, this means for small molecules, the DEP penetration into a microchannel will be diminishingly small. To effectively extend the penetration of the DEP force, electrothermally generated fluid circulation can be combined with DEP. The electrothermal force circulates the fluid, and the suspended antigen, passing it within close range of the DEP electrodes, where they can be captured by the short-range DEP. Once a concentration has built up on the DEP electrodes, these electrodes can be cycled off to release the antigen to the binder.

The finite element package Femlab was used to solve the particle velocity field, balancing fluid drag with DEP force for steady state motion. This DEP model is combined with the electrothermal model presented above. Results of this combined model are shown in Fig. 17, which represents the concentration of antigen suspended in the channel, before (a) and after (b) the DEP electrodes are turned off. Figure 18 shows the DNA binding rates as a result of DEP focusing. The binding rate is increased by approximately 55% using DEP.

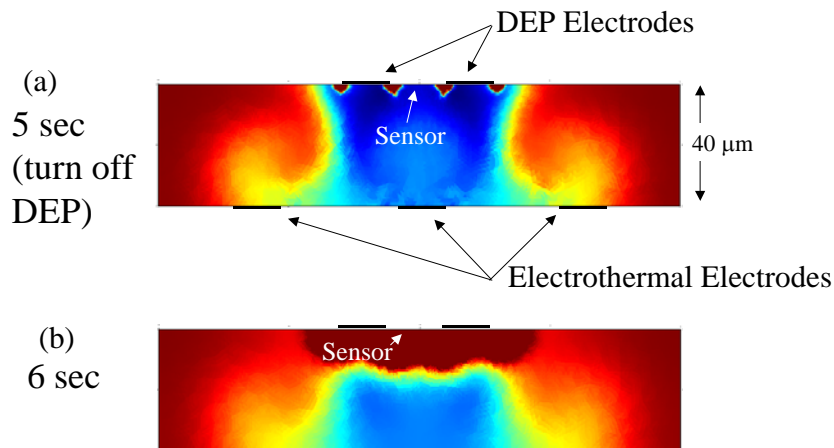


Figure 17. Electrothermal electrodes at one frequency create circulating motion of the fluid, while DEP electrodes at a different frequency capture suspended molecules. The red color near the electrode edges in (a) shows a concentration building up. In (b) the electrodes have been turned off, and the concentration has been released. A concentrated cloud now surrounds the sensor (binder).

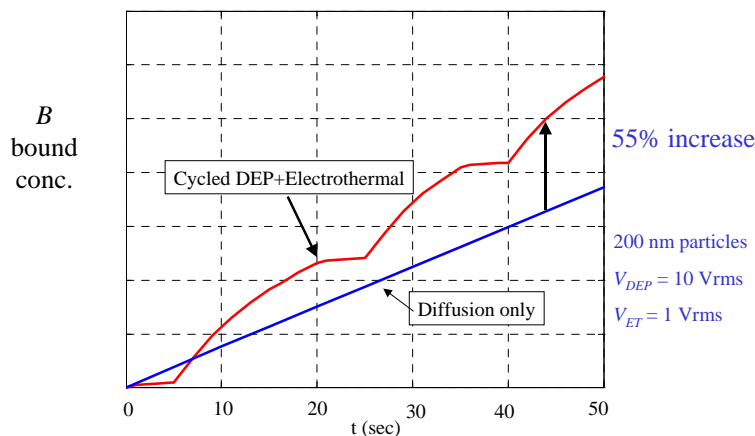


Figure 18. Binding rate for model shown in Fig. 17. DEP and Electrothermal flow increases the binding rate about 55%.

#### 4.3.4 Summary

We have demonstrated two AC electrokinetics tools that can be used independently, or in conjunction with each other, to improve existing heterogeneous assays. By designing a microchannel electrode system that takes advantage of electrothermal effects, cross-stream transport of an antigen and hence binding can be enhanced. Numerical simulations predict factors of 2~8 improvement; with electrode and heat transfer optimization, an order of magnitude increase in binding rate may be achieved. This enhancement technique can be applicable to a wide variety of assay formats. With the addition of DEP for concentrating molecules, even reaction limited binding assays may be improved.

#### 4.4 Surface Chemistry Development

During the first quarter of the project, it was established that either  $\text{SiN}_x$  or  $\text{SiO}_2$  could be deposited onto the tunable laser prior to chemical immobilization. Immobilization onto these types of surfaces has been proven feasible with peptides by groups at UCSB (Whaley, 2000) that demonstrated immobilization onto single crystal semiconductor surfaces ( $\text{GaAs}(100)$ ,  $\text{GaAs}(111)$ ,  $\text{InP}(100)$ , and  $\text{Si}(100)$ ) and though the use of aryldiazirin-based molecules by a group in Switzerland (Gao, 1995; Gao, 1997) that immobilized biomolecules onto  $\text{SiO}_2/\text{TiO}_2$  and  $\text{SiN}_x$  surfaces. Here, a series of experiments was carried out incorporating two model chemistry systems consisting of two different photolinkers conjugated to fluorescent labels, the immobilization procedures presently used at ThauMDx, and a modified washing process following Gao et al. for immobilizing chemistry to a surface. The first photolinker molecule examined was a photoreactive psoralen and the second photolinker was a nitrophenyl azide based molecule. The conjugates were deposited onto  $\text{SiN}_x$  coated Si wafers and  $\text{SiO}_2$  glass cover slips from Fisher Scientific. The substrates were then treated with curing steps from the process presently used at ThauMDx and washing steps modified from Gao. By examining the fluorescence of these treated samples, we can establish the optimal photolinker to use in conjunction with the coated TLCS surface as well as the immobilization process which yields the strongest bound chemistry. Unfortunately, analysis of these systems demonstrated that binding via these two types of linker molecules does not adequately bind the antibody chemistry to the TLCS surface.

We examined immobilization of biomolecules using silane surface treatment reagents. The chemical structure of the silane presently being tested is shown in Figure 19. Binding of this molecule to a surface containing silicon results in a surface activated with a primary amine functional group (Hermanson, 1992). The primary amine functional group can then be reacted with the biomolecule to be immobilized thus fixing the biomolecule to the surface of interest. The binding strength of the silane was evaluated with  $\text{SiO}_2$  glass cover slips from Fisher Scientific and  $\text{SiN}_x$  coated Si wafers from Dan Cohen. Preliminary experiments demonstrate that the binding strength of the silane to either  $\text{SiN}_x$  or  $\text{SiO}_2$  is considerably greater than that seen with the original photolinkers tested. Due to the success seen in these systems, we are now initiating immobilization experiments with the silane chemistry on  $\text{SiN}_x$  and  $\text{SiO}_2$  coated InO in order to better mimic the environment of the TLCS.

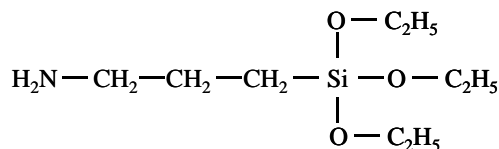


Figure 19: Chemical structure of the 3-aminopropyltriethoxysilane (Pierce Endogen). The silane will bind to surfaces containing silicon atoms while the primary amine can be used to react with the biomolecule of interest to immobilize the molecule to the surface.

#### 4.4.2 Experiments: Immobilization on $\text{SiO}_2$

Objective:

The goal of this effort is to develop a protocol for immobilization of proteins on the  $\text{SiO}_2$ -covered wafer surface for use in analytical detection of biological targets in evanescent field instrumentation. Ideal method would produce a thin layer of stable, active, immobilized antibodies competent of specific and efficient antigen binding.

## Materials:

APTES (3-aminopropyltriethoxysilane), MPTS (3-mercaptopropyltrimethoxy silane), and BIO-CONEXT (trimethoxy silane aldehyde) were tested as means for activation of the SiO<sub>2</sub> surface. These silanes differ by the reactive group available for cross-linking: APTES contains –NH<sub>2</sub> group, MPTS has –SH group, and BIO-CONEXT has -CHO group. Additionally, covalent cross-linkers such as glutaraldehyde, GMBS, and MPBA were tested.

Preliminary studies were done using microscope slides as a model surface. Fisher premium brand microscope slides were selected for this purpose since they produced the lowest background of non-specific adsorption. Selected conditions for antibody immobilization were further tested on SiO<sub>2</sub>-covered wafers.

Goat anti-glucose oxidase antibodies and glucose oxidase from *A. niger* were used as model antibody and antigen respectively. Specific affinity of this antibody-antigen pair was confirmed by in-gel immunoprecipitation. Either protein could be labeled with NBD-X (succinimidyl 6-(*N*-(7-nitrobenz-2-oxa-1,3-diazol-4-yl)amino)hexanoate) fluorescent dye from Molecular Probes when necessary for detection and quantitative measurement purposes.

## Methods:

The silanes were deposited and cured according to the manufacturer recommendations. APTES treated slides were activated with glutaraldehyde. BIO-CONEXT silanized surfaces were used without further treatments. MPTS modified surfaces in some instances were additionally treated with GMBS, or DTT as required, or the protein to be immobilized was pre-activated with MPBA. Antibodies were applied to the modified surfaces for various times and at different concentrations and buffer conditions. Unreacted antibodies were washed off with PBS-Tween 20 buffer. Surface was blocked with instant milk, unrelated IgGs, or BSA. At the next step, solution of the antigen in PBS buffer was applied to the activated surface and incubated for various times and at different concentrations. The antigen was labeled with fluorescent dye to facilitate the detection and analytical measurements. Finally, the unbound labeled antigen was washed off with PBS-Tween 20 buffer and slides were dried. For quantitation of antibody immobilization, IgGs were labeled with NBD-X directly. Fluorescence was detected using Molecular Dynamics Phosphoimager 840, and label retention was analyzed using ImageQuANT software.

## Results

### A. Development of immobilization procedure on glass slides.

Image presented on Figure 20 demonstrates that anti-glucose oxidase antibodies can be immobilized on the SiO<sub>2</sub> surface, and that these cross-linked antibodies maintain the ability to bind antigen (NBD-X conjugated glucose oxidase). The best antibody-mediated capture of the antigen is achieved on MPTS modified surface. MPTS-treated slide shows both the lowest background antigen adsorption and high antibody-mediated antigen retention. Capture of the antigen was specific, as it was not affected by commonly used suppressors of non-specific binding such as BSA, casein, unrelated IgG, or instant milk, but was efficiently competed out by unlabeled glucose oxidase (data not shown). As the concentration of antibodies applied to MPTS-modified glass surface was increased, the amount of antibodies immobilized increased as well, reaching saturation at approximately 200 ng/cm<sup>2</sup> (data not shown). This antibody surface density is similar to the results reported by others (1-4). It should be noted that higher density would not necessarily result in more efficient antigen binding due to potential steric hindrance and inactivation of antibodies. Importantly, data indicate that antibodies immobilized on glass surface retain up to 35% of their activity, which is also well within expectations (1-3, 5). Binding of antigen to immobilized antibody had only limited dependence on the length of incubation (data not shown), suggesting that measurements in this assay format can be done quickly.

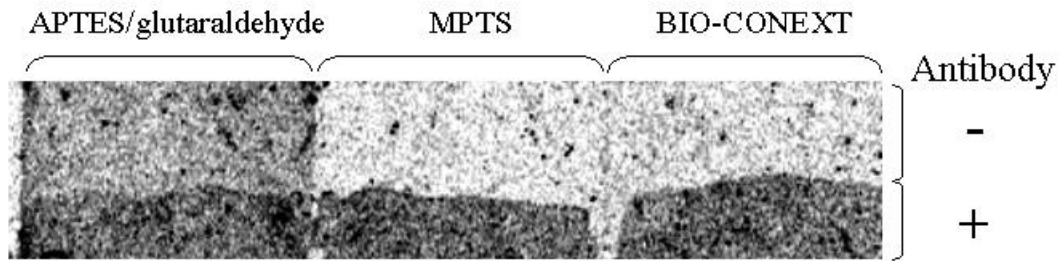


Figure 20. Visualization of antibody-mediated capture of fluorescent antigen on silane-modified glass surface. Fluorescent antigen retained on the surfaces of slides treated with indicated silanes. Bottom portion of each slide was loaded with anti-glucose oxidase antibodies from 0.5 mg/ml solution, slides were washed and incubated in the 0.01 mg/ml solution of NBD-X conjugated glucose oxidase. Excess of the antigen was washed off and retained fluorescence was detected using Molecular Dynamics Phosphoimager 840.

### B. Immobilization of active antibodies on SiO<sub>2</sub> covered wafers

Having proven that we are capable of immobilizing active antibodies on the glass surface we applied the described protocol to SiO<sub>2</sub>-covered wafers. APTES, BIO-CONEXT, and MPTS silanes were tested in combination with appropriate cross-linkers. Best results were obtained using MPTS surface activation and GMBS cross-linker. Efficiency of antibody immobilization depended on the thickness of the SiO<sub>2</sub> film (Fig. 21).

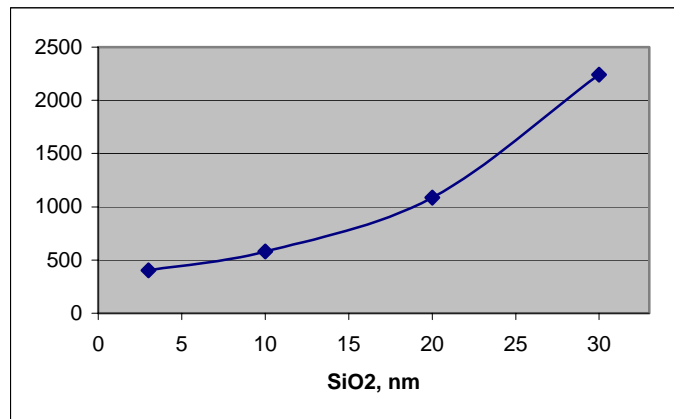


Figure 21. Immobilization of antibodies on the wafers with different thickness of SiO<sub>2</sub> layer. NBDx-labeled IgGs were applied to wafer fragments activated with MPTS silane and MPBA cross-linker, unreacted IgGs were washed off, and immobilized fluorescent signal was measured.

Effect of increasing the salt (NaCl) concentration on immobilization of IgGs (Fig. 22) suggests that it is the charged surface of the wafer that is inhibitory for the antibody immobilization. As the thickness of SiO<sub>2</sub> film is increasing, so does the distance between charged surface and the antibody being immobilized. Thus, the inhibitory effect of the charge is reduced. However, the penetrating ability of the evanescent field that is the key for the application is expected to limit the thickness of the SiO<sub>2</sub> layer that can be used. Salt is apparently capable to partially relieve the inhibition by shielding the charges.

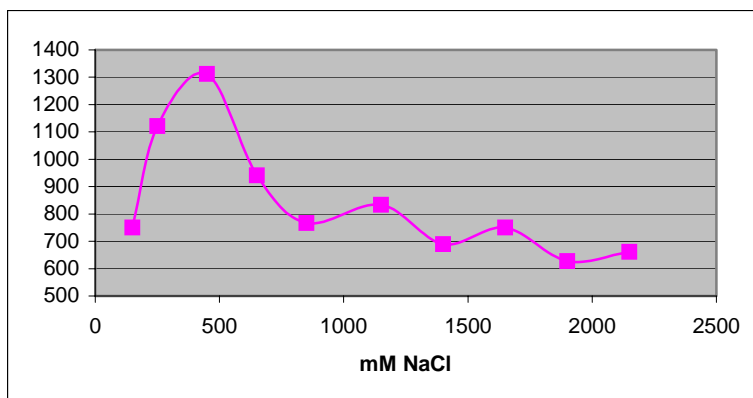


Figure 22. Effect of NaCl concentration on immobilization of antibodies on the 10 nm SiO<sub>2</sub>-covered P-type wafer.

Optimal pH for antibody immobilization was found to be between 6 and 7 (Fig. 23). Temperature did not significantly affect the immobilization efficiency (data not shown).

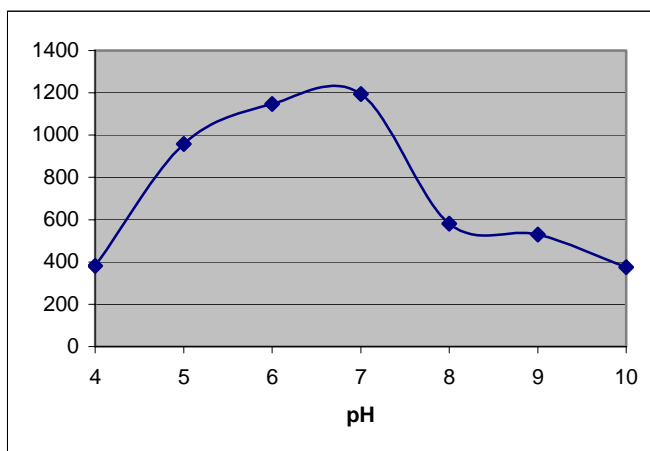


Figure 23. Effect of pH on immobilization of antibodies on the 10 nm SiO<sub>2</sub>-covered P-type wafer. Quantitation was performed as described in the legend for Figure 12.

Under optimal conditions up to 150 ng/cm<sup>2</sup> of antibody could be immobilized on P-type wafers with 10 nm SiO<sub>2</sub> layer. Activity of antibodies immobilized on SiO<sub>2</sub>-covered wafers is noticeably lower than that on the glass slides (10-15% vs. 30-35%) (data not shown). The exact cause for that has not yet been determined. However, this activity may still be sufficient. Simple quantitation shows that antibody density of 150 ng/cm<sup>2</sup> results in about 6x10<sup>11</sup> IgG molecules/cm<sup>2</sup>. Even at only 10% activity, they can still bind 12x10<sup>10</sup> molecules of antigen/cm<sup>2</sup>. For an average protein antigen (molecular weight of 150 kDa), 1 cm<sup>2</sup> of such surface can theoretically bind 30 ng of the antigen, or all the antigen molecules from 0.1 ml of solution with concentration of 300 ng/ml, which is significantly higher than the target sensitivity of the final application. These numbers mean that sheer quantity of immobilized antibodies is unlikely to be the limiting factor for the final application.

The protocol for the immobilization of active antibodies on the SiO<sub>2</sub>-covered wafer surface modified with silanes has been developed. This procedure can now be used to immobilize antibodies on the waveguides.

#### 4.4.4 Methods of Chemistry Deposition

Another challenge for chemistry development for the TLCS is the physical deposition of the biochemistry onto the TLCS sensing region. Due to the small area allowable for the sensing region (3 μm X 100 μm), the biochemistry cannot be deposited using the biodot system presently in use at ThauMDx. Instead, a micro

deposition system must be used. There are many different types of methods of micro deposition which may be compatible for use with the TLCS. These include self-aligning techniques, masking processes, and precise deposition via systems such as quills or polydimethylsiloxane (PDMS)-stamps.

The exact method used to deposit chemistry onto the surface of the TLCS is dependent upon the surface topology of the TLCS where chemistry deposition is desired. However, for our application, the precise deposition methods via systems such as quills or PDMS-stamps are most viable.

If the surface is flat, the PDMS stamp method would be an optimal method for depositing chemistry precisely, both spatially and quantitatively. PDMS is a commonly used polymer for transfer of biomolecules due to its elastomeric properties and its biocompatibility (Kane, 1999). The PDMS-stamp is prepared by casting a liquid prepolymer of the PDMS against a master which has a patterned relief structure. The master is often fabricated out of a Si wafer using lithography techniques. For applications on the TLCS, we have chosen to prepare a stamp with a patterned structure of ridges 3 microns wide spaced 150 microns apart. These dimensions mimic the dimensions required for transfer of biochemistry onto the TLCS with the PDMS-stamp technique. Using a mask supplied by Dan Cohen, Kimberly Turner has prepared a master from an Si wafer which contains 3 micron wide troughs spaced 150 microns apart. The master is shown in Figure 11A-B. A PDMS-stamp will be cast and set using this master. Once the stamp is prepared, transfer of biomolecules from a solution to a solid substrate is obtained by dipping the stamp into the solution (“inking” the stamp) and then “stamping” the chemistry onto a solid substrate. The stamp will be tested for reproducibility in transferring a defined amount of chemistry from a solution to a solid substrate.

As an example of the precision obtained with the PDMS stamping technique, a PDMS-stamp was cast from a master containing 3 micron wide troughs spaced 6 microns apart center-to-center (Figure 24C). Each trough was approximately 1 cm long. A PDMS-stamp was cast against this master to create a stamp with 3 micron wide ridges. The stamp was then used to transfer fluorescently tagged lipid molecules from a solution to a glass cover slip. The results are shown in Figure 3D. The light areas are areas that contain lipid transferred to the cover slip while the dark areas are void of lipid. It is readily apparent that the dimensions of the PDMS-stamp were retained to a high degree.

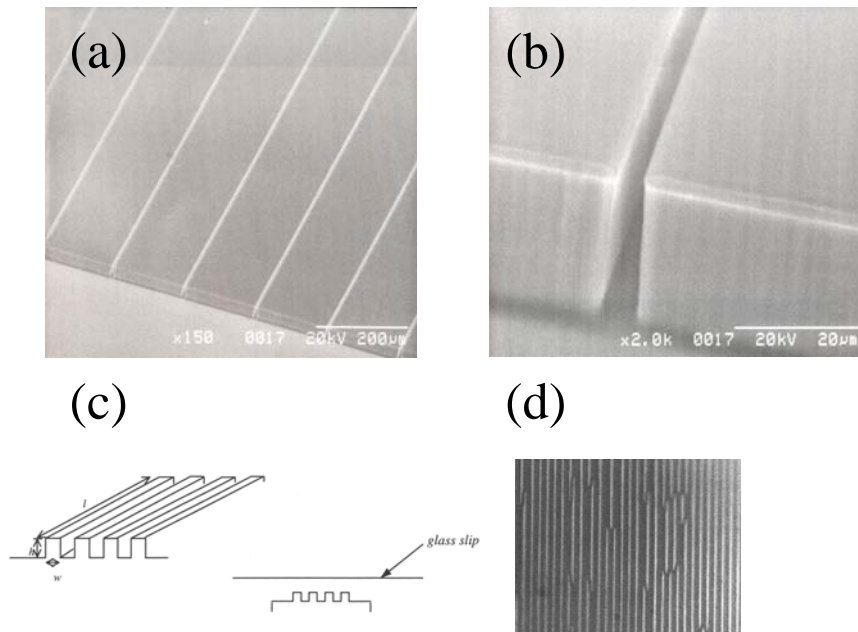


*Figure 24:* (a.) Scanning electron microscopy (SEM) micrograph of the PDMS master fabricated by Kimberly Turner from a Si wafer at 150 times magnification. The white lines are 3 micron wide troughs. (b.) SEM micrograph of the same PDMS master at 2000 times magnification highlighting the 3 micron wide trough. (c.) A schematic drawing of a sample PDMS-stamp with dimensions  $w=3$  microns,  $h \sim 2.5$  microns,  $l \sim 1$  cm. The 3 micron wide ridges are separated by 6 microns center-to-center. Also demonstrated is how the stamp was used to transfer biomolecules to a glass cover slip. (d.) Optical micrograph of fluorescently labeled lipids transferred to a glass cover slip with the sample PDMS-stamp. Light regions contain the fluorescently labeled lipid and dark regions are void of lipid. The lines are 3 microns wide. This micrograph demonstrates the precision of deposition of biomolecules with the PDMS-stamp.

## Conclusions

We have developed and demonstrated that integrated InP lasers can in principle be used as a bio-molecular sensor. In order for the lasers to have acceptable sensitivities, the laser must be designed to optimize for high mode overlap. We show that a symmetric waveguide approach shows the most promise and can increase mode overlap to approximately 4%.

The concept of using ac electrokinetics (i.e. the electrothermal effect & dielectrophoresis) to enhance immunoassay binding and bio-molecular focusing has been developed in this research. We used numerical simulations to show that immunoassay binding rates can be improved by a factor of 8, using 14 Vrms potential.

A significant challenge of this project is the ability to attach antibodies to the InP laser structure. We demonstrated that antibodies can be attached to a 30 nm layer of SiO<sub>2</sub> is deposited on the InP substrate. However, if the SiO<sub>2</sub> layer is significantly reduced, the antibodies are not well attached. The 30 nm thick SiO<sub>2</sub> layer is not desirable, because it will significantly reduce mode overlap, thereby decreasing the laser sensitivity. A PDMS stamp is shown to be an excellent technique for selectively depositing antibodies on the laser structure.

## References

- Cohen, D.A, J. A. Nolde, A. Tauke Pedretti, C. S. Wang, E. J. Skogen, L. A. Coldren, "Sensitivity and scattering in a monolithic heterodyned laser biochemical sensor," *IEEE Journal of Selected Topics in Quantum Electronics*, vol. 9, pp.1124-1131, 2003.
- Cohen, D.A., E. J. Skogen, H. Marchand, and L. A. Coldren, "Monolithic chemical sensor using heterodyned sampled grating DBR lasers," *Electronics Letters*, vol. 37, pp. 1358-1360, 2001. Gao et al (1995), Immunosensing with photoimmobilized immunoreagents on planar optical wave guides. *Biosensors and Bioelectronics*, **10**: 317-328
- Gao et al (1997) Bioengineering of silicon nitride. *Sensors and Actuators B*, **38-39**: 38-41
- Hermanson, et. al. (1992) Immobilized Affinity Ligand Techniques, Academic Press, Inc., San Diego CA., 12-14.
- Kane et al (1999) Patterning proteins and cells using soft lithography. *Biomaterials*, **20**: 2363-2376
- Meinhart, C.D., S.T. Wereley, and J.G. Santiago *PIV Measurements of a Microchannel Flow*. Exp. in Fluids, Vol. 27, pp. 414-419, (1999).
- Miles, R., P. Belgrader, K. Bettencourt, J. Hamilton, S. Nasarabadi, *Dielectrophoretic manipulation of particles for use in microfluidic devices*, MEMS-Vol. 1, Microelectromechanical Systems (MEMS), Proceedings of the ASME International Mechanical Engineering Congress and Exposition, Nashville, TN, Nov. 14 – 19, (1999).
- Myszka, D.G. 1998. Survey of the 1998 optical biosensor literature. *J Mol. Recognit.* Vol. 12, pp. 390-408.
- Ramos, A., Morgan, H., Green, N.G., and Castellanos, A., *Ac electrokinetics: a review of forces in microelectrode structures*, *J. Phys. D: Appl. Phys.* Vol. 31, pp. 2338-2353, (1998).
- Wang, C.S., J. A. Nolde, D. D. Lofgreen, L. A. Coldren, D. A. Cohen, "A self-aligned process to monolithically integrate a quasi-symmetrical sensing waveguide to a diode laser chemical sensor," submitted to *Applied Physics Letters*, 2004.
- Whaley et al (2000) Selection of peptides with semiconductor binding specificity for directed nanocrystal assembly. *Nature*, **405**: 665-668
- Yang, J., Huang, Y., Wang, X-B, Becker, F., and Gascoyn, P., *Cell separation on microfabricated electrodes using dielectrophoretic/gravitational field-flow-fractionation*, *Anal. Chem.*, Vol. 71, pp. 911-918, (1999)

## 5. Technology Transfer

We are continuing our efforts to investigate potential commercial applications resulting from this research with *Agility Communications*. *Agility Communications* is also a startup company in Santa Barbara who is developing widely tunable SGDBR lasers with control boards for communication and sensing systems. Currently, our technology has not been developed sufficiently to warrant commercialization.